Effect of the Combination of Different Electrode Spacings and Power on Bipolar Radiofrequency Fat Dissolution: A Computational and Experimental Study

Lianru Zang, Yu Zhou,* Jia Kang, and ChengLi Song
Shanghai Institute for Minimally Invasive Therapy, University of Shanghai for Science and Technology, 516 Jungong Road, 200082, Shanghai, China

Background and Objectives: The finite element method was used, and experiments were performed to analyze the effect of different electrode spacings and power combinations on the electrical and thermal aspects of biological tissues during bipolar radiofrequency (RF) fat dissolution. Through these efforts, this study also attempted to develop a reasonable electrode spacing and power combination that can achieve fat dissolution effects, the RF energy of which will not thermally damage the tissue.
Study Design/Materials and Methods: COMSOL was adopted to conduct a finite element analysis for bio-thermoelectric coupling, and a two-dimensional time-domain model of biological tissue was built. A self-developed single-channel bipolar RF device was employed to load RF energy on the *ex vivo* porcine abdominal tissue. The thermal characteristics of the tissue were characterized and analyzed with a thermal imager and thermocouple probes.
Results: Under a power of 5 W combined with the electrode spacings of 1, 2, and 3 cm, the temperature in the tissue could not reach that required for fat dissolution. Under a power of 15 W combined with the electrode spacings of 1, 2, and 3 cm, the RF energy would thermally damage part of the skin areas. Besides this, the combination of a power of 10 W and the electrode spacing of 1 cm would thermally damage the skin areas. The combination of a power of 10 W and the electrode spacing of 2 or 3 cm made part of the fat layer of the tissue satisfy the requirements of fat dissolution, and the fat dissolution area caused by the former was 118% larger than that of the latter; in the meantime, no heat damage to the skin layer was found.
Conclusion: Different electrode spacings and power combinations significantly affect the electrical and thermal properties of bipolar RF energy loaded on biological tissue, a reasonable electrode spacing and power combination is one of the critical factors leading to the success of bipolar RF fat dissolution. Lasers Surg. Med. © 2020 Wiley Periodicals, Inc.

Key words: bipolar radiofrequency; fat dissolution; finite element analysis; electrode spacing; constant power; hyperthermia

INTRODUCTION

Public awareness of the health problems attributed to obesity has been growing, and it is increasingly accepted that having a thinner body is a sign of beauty. As these two developing consciousnesses have become instilled in the public, we yearn being thinner and healthier. The rising demand for fat dissolution has also created a considerably huge beauty and body shaping market.

Thus far, four major non-invasive technologies have been extensively adopted to reduce fat, namely, radio-frequency (RF), low-level laser therapy, high-intensity-focused ultrasound, and cryolipolysis [1]. RF has been widely employed in body shaping, fat dissolution, and skin tightening [2]. RF is well accepted for its non-invasive and selective ability to heat target tissues without impairing the surrounding tissues, creating a unique advantage for non-invasive selective heating of subcutaneous adipose tissue. RF current is capable of causing irreversible thermal damage to adipose tissue by directionally regulating the generation of the electric field in the tissue. Fifteen minutes *in vivo* thermal exposures to 43–45°C could lead to the formation of a delayed adipocyte cellular death response [3], so increasing the temperature of adipocytes and maintaining it above the threshold of apoptosis can induce apoptosis, which reduces the number of adipocytes and the volume of fat.

The types of RF devices include monopolar, bipolar, and multipolar. The monopolar system shows a defect in that its behavior is unpredictable when the current flows through the body to the grounding electrode. Kaplan and Gat [4] reported that when the monopolar system was adopted for fat reduction, temporary erythema, edema after treatment, purpura, pigmentation after inflammation, subcutaneous erythema papules, blisters,

Conflict of Interest Disclosures: All authors have completed and submitted the ICMJE Form for Disclosure of Potential Conflicts of Interest and none were reported.
*Correspondence to: Yu Zhou, PhD, Shanghai Institute for Minimally Invasive Therapy, University of Shanghai for Science and Technology, 516 Jungong Road, 200082 Shanghai, China. E-mail: zhouyu_working@163.com
Accepted 16 April 2020
Published online in Wiley Online Library (wileyonlinelibrary.com).
DOI 10.1002/lsm.23256

and superficial burns would appear. The bipolar systems exhibit the merit that the direction of the current is controllable, so the current is concentrated in the area between the positive and the negative. Accordingly, the RF energy can be more concentrated, and unnecessary damage to other tissues caused by the spread of the current can be avoided. In the bipolar system, the penetration depth of the current is less than that of monopolar [5,6], suggesting that the RF energy reaches the subcutaneous fat with more difficulty. The electrode distance affects current density in tissues, and the current density is a vital parameter affecting tissue temperature variation [7]; besides this, researchers considered that different parameters also show associations with RF success (e.g., frequency and device power, treatment time and temperature maintained in the skin), whereas no relevant definitive agreement has been reached [8].

This study aimed to delve into the effects of electrode spacing and RF power, two necessary parameters, on bipolar RF fat dissolution and attempted to exploit their combination. It was expected that RF energy could be applied to the fat layer in bipolar mode to achieve practical fat dissolution while protecting the skin layer from thermal damage to the greatest extent.

MATERIALS AND METHODS

Governing Equations

As electrical propagation is speedy compared with the thermal diffusion, it was assumed to be time-independent. This study exploited a quasi-static formula to simulate the response of the tissue to the electric field, indicating that the spatial distribution of the electromagnetic field in the range of the device was identical to that of the electrostatic field [9]. There was no other RF source inside the biological tissue, so its potential was regulated by the Laplace equation [10].

$$\nabla \cdot (\sigma_i \nabla V_i) = 0 \tag{1}$$

the sub-index i denotes the epidermis, dermis, fat, fibrous septa, or muscle, $i = \{e, d, f, fs, m\}$, respectively. Where σ(S/m) is the electric conductivity, and V is the voltage in the tissue.

In biological tissues, the energy dissipation rate per unit volume at a given point was proportional to the electric conductivity of the tissue and the square of the induced internal electric field [11]:

$$Q_i = \sigma_i \|E_i\|^2/2 \tag{2}$$

where Q(W/m^3) denotes the electric power absorption.

The physical phenomena of the thermoelectric coupling problem complied with the Pennes biological heat transfer equation [12]:

$$\rho_i c_i \frac{\partial T_i}{\partial t} = \nabla \cdot (k_i \nabla T_i) + \rho_b c_b \omega_i (T_b - T_i) + Q_i + Q_m \tag{3}$$

where ρ(kg/m^3) is the density, c(J/kg/K) is the specific heat, k(W/m/K) is the thermal conductivity, T is the temperature in K, ρ_b(kg/m^3) is the blood density, c_b(J/kg/K) is the blood specific heat, ω(kg/m^3/s) represents the blood perfusion rate, T_b is the arterial temperature in K, Q(W/m^3) is the power absorption, and Q_m(W/m^3) is the metabolic heat generation. As the contribution of the Q_m is obviously smaller than other terms, it is neglected [13].

Domain and Boundary Conditions

Domain. In this multi-layer model, the skin is considered a two-layer structure consisting of the epidermis and dermis. The area of the model is expressed as $W \times L$, where W is the overall width and L is the overall depth composed of L_e, L_d, L_f, L_m. The diameter of the electrode head is expressed as W_p. For clinical relevance, the original fibrous septa configuration was extracted from a micro-magnetic resonance imaging (MRI) image [14] and then substituted into the fat layer of the model. The geometric structure of the model is shown in Figure 1; the geometric dimensions of the model are listed in Table 1. The rationality of the size of the model was assessed as follows:

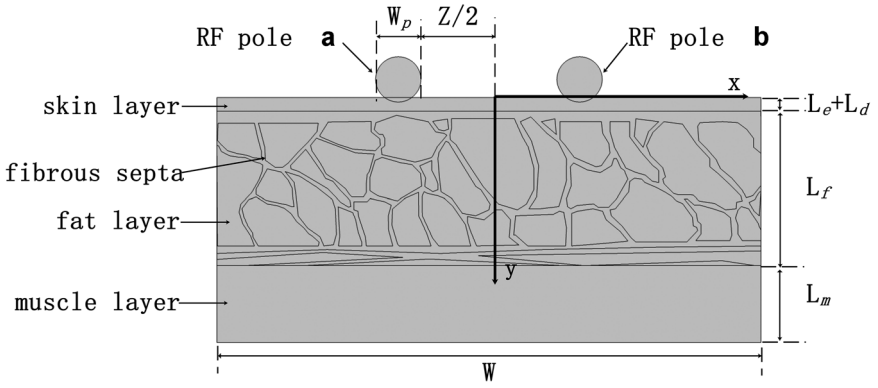

Fig. 1. Tissue layers of epidermis, dermis, fibrous septa structures, fat, muscle, and RF poles. RF, radiofrequency.

TABLE 1. Model Geometry

Parameter	Value (mm)
W	60
W_p	5
L_e	0.1
L_d	1.5
L_f	17
L_m	8.5

- The thickness of the subcutaneous fat varied significantly with the individual; to fit the experiment, the thickness of the subcutaneous fat was measured in five *ex vivo* porcine tissues applied in the experiment and an average was obtained, which was set as the value of L_f.
- The density of the fibrous septa network architecture also varied significantly with the individual. In this model, an example of the intermediate fibrous septa network architecture was employed. Ana et al. [15] analyzed an intermediate-density and a high-density fibrous septa network architecture by an identical RF treatment; the result suggested that their temperature distributions at steady-state ($t = 8000$ seconds) were similar.
- To simulate the effect of slight electrode pressure on the skin, the depth of electrode contact with the skin layer was set to 0.5 mm in the model.

Boundary Conditions

Electrical boundary conditions. The RF voltage $V = \sqrt{PZ}$ was loaded on electrode "b," and the zero voltage was loaded on the other electrode "a," where P denotes the power of the RF device, Z is the value of bioimpedance, which is obtained with an impedance analyzer (IM3570; HIOKI, Ueda-Shi, Japan) to ascertain the impedance of the *ex vivo* porcine abdominal tissue at 450 kHz and different electrode spacings. The residual epidermis area, the muscle bottom area, and the lateral boundaries referred to the zero electric flux conditions. At the time $t = 0$, it was assumed that $V = 0$.

Thermal boundary conditions. This study defined the skin area between the two electrodes as the skin-gel contact surface and set the residual skin area as the air-skin contact surface. The corresponding surface heat dissipation coefficient h_i was applied, where $i = \{a, g\}$ on the two contact surfaces to simulate the cooling effect generated by airflow or gel, the heat dissipation coefficient of skin-gel contact h_g is 1200 W/m^2/K, and that of tair-skin contact h_a is 10 W/m^2/K. The residual boundary referred to the zero thermal flux condition. At $t = 0$ the temperature of the tissue T_0 was 310 K, the environment temperature T_{ext} was 293 K, and the blood temperature T_b was 310 K. Figure 2a and b illustrate the electrical and thermal boundary conditions of the model, respectively, and a summary of the conditions is presented in Table 2.

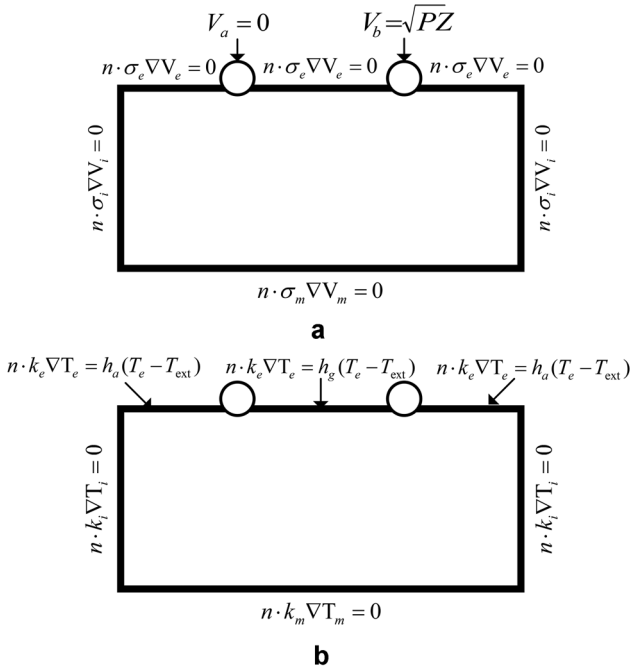

Fig. 2. The electrical and thermal boundary conditions of the model. (**a**) Electrical boundary; (**b**) Thermal boundary.

Thermal Damage

Thermal damage is considered a first-order kinetic process, calculated by the Arrhenius equation [16,17], which relates cell activity to exposure time and temperature as expressed below:

$$\Omega(\tau) = \ln\left\{\frac{C(0)}{C(\tau)}\right\} = \int_0^\tau A e^{\frac{-E_a}{RT(t)}} dt \tag{4}$$

where $\Omega(\tau)$ denotes the logarithm of the ratio of initial concentration $C(0)$ to actual concentration $C(\tau)$, τ is the heating time in s, A is the frequency factor in (1/s), E_a is the activation energy for an irreversible reaction in (J/mol), and R represents the universal gas constant. From experiments of skin heating in the 44–50°C temperature range, $A = 2.185 \times 10^{124}\,\text{s}^{-1}$ and $\Delta E = 7.82 \times 10^5$ J/mol, when the temperature reaches over 50°C, $A = 1.823 \times 10^{51}\,\text{s}^{-1}$ and $\Delta E = 3.27 \times 10^5$ J/mol [18]. The contours of $\Omega = 1$ represent a 63% decrease in viability.

Physical Assumptions for Modeling

Tissues were assumed as isotropic materials; the distribution of blood vessels was assumed to be isotropic. Physical properties of fibrous septa were assumed to be similar to the dermis as it is a collagenous tissue and an extension of the dermis [11]. Variations in thermal conductivity (in the 30–48°C range, pig epidermis: 0.16–0.25 W/m/K, pig dermis: 0.36–0.38 W/m/K, pig subcutaneous fat: 0.15–0.17 W/m/K [19]), and specific heat (in the 25–80°C range about 0.3% deviation from average value [20]) were insignificant, so the thermal conductivity and specific heat value were assumed to be constant.

TABLE 2. Electric and Thermal Boundary Conditions

Location	Electric	Thermal
Skin surface ($y = 0$)	$\{n\cdot\sigma_e\nabla V_e = 0 \mid -W/2 < x < -Z/2 - W_p\}$	$\{n\cdot k_e\nabla T_e = h_a(T_e - T_{ext}) \mid -W/2 < x < -Z/2 - W_p\}$
	$\{V_a = 0 \mid -Z/2 - W_p < x < -Z/2\}$	$\{n\cdot k_e\nabla T_e = h_g(T_e - T_{ext}) \mid -Z/2 < x < Z/2\}$
	$\{n\cdot\sigma_e\nabla V_e = 0 \mid -Z/2 < x < Z/2\}$	$\{n\cdot k_e\nabla T_e = h_a(T_e - T_{ext}) \mid Z/2 + W_p < x < W/2\}$
	$\{V_b = \sqrt{PZ} \mid Z/2 < x < Z/2 + W_p\}$	
	$\{n\cdot\sigma_e\nabla V_e = 0 \mid Z/2 + W_p < x < W/2\}$	
Between layers ($y = -L_e$)	$\{n\cdot\varepsilon_0\varepsilon_{rs}E_e = n\cdot\varepsilon_0\varepsilon_{rs}E_d \mid -W/2 < x < W/2\}$	$\{n\cdot k_e\nabla T_e = n\cdot k_d\nabla T_d \mid -W/2 < x < W/2\}$
	$\{V_e = V_d \mid -W/2 < x < W/2\}$	$\{T_e = T_d \mid -W/2 < x < W/2\}$
Between layers ($y = -L_d$)	$\{n\cdot\varepsilon_0\varepsilon_{rs}E_d = n\cdot\varepsilon_0\varepsilon_{rs}E_f \mid -W/2 < x < W/2\}$	$\{n\cdot k_d\nabla T_d = n\cdot k_f\nabla T_f \mid -W/2 < x < W/2\}$
	$\{V_d = V_f \mid -W/2 < x < W/2\}$	$\{T_d = T_f \mid -W/2 < x < W/2\}$
Between layers ($y = -L_f$)	$\{n\cdot\varepsilon_0\varepsilon_{rs}E_f = n\cdot\varepsilon_0\varepsilon_{rs}E_m \mid -W/2 < x < W/2\}$	$\{n\cdot k_f\nabla T_f = n\cdot k_m\nabla T_m \mid -W/2 < x < W/2\}$
	$\{V_f = V_m \mid -W/2 < x < W/2\}$	$\{T_f = T_m \mid -W/2 < x < W/2\}$
Muscle bottom ($y = -L_m$)	$\{n\cdot\sigma_m\nabla V_m = 0 \mid -W/2 < x < W/2\}$	$\{n\cdot k_m\nabla T_m = 0 \mid -W/2 < x < W/2\}$
Left side ($x = -W/2$)	$\{n\cdot\sigma_i\nabla V_i = 0 \mid -L < y < 0\}$	$\{n\cdot k_i\nabla T_i = 0 \mid -L < y < 0\}$
Right side ($x = W/2$)	$\{n\cdot\sigma_i\nabla V_i = 0 \mid -L < y < 0\}$	$\{n\cdot k_i\nabla T_i = 0 \mid -L < y < 0\}$

Blood perfusion is critical to the heat transfer in tissue [21]; the rate of blood perfusion was assumed to be a temperature-dependent piecewise function and taken as follows [22]:

(i) Blood perfusion in the dermis

$$\omega_d = \omega_0(1 + \gamma T) \tag{5}$$

where ω_0 and γ denote the baseline blood perfusion and the linear coefficient of temperature dependence, respectively.

(ii) Blood perfusion in the fat

$$\omega_f = \begin{cases} 0.36 + 0.36e^{-(T-45)^2/12} & T \le 45 \\ 0.72 & T > 45 \end{cases} \tag{6}$$

(iii) Blood perfusion in the muscle

$$\omega_m = \begin{cases} 0.45 + 3.55e^{-(T-45)^2/12} & T \le 45 \\ 4 & T > 45 \end{cases} \tag{7}$$

Biological tissues exhibited several different dispersions over a wide range of frequencies [23]. To comply with the experimental conditions, the electric conductivity and permittivity used in this study corresponded to 450 kHz. The physical properties of each part of the model are listed in Table 3.

Ex Vivo Experimental Method

Ex vivo experiments were performed with a self-developed single-channel bipolar RF device. The device could produce a 450 kHz sine wave, as isolated by a transformer and connected to two stainless steel electrodes with a diameter of 5 mm that contacted the tissue; the device detected the impedance variations in tissue in the experiment and employed the PID algorithm according to the current biological impedance value to rapidly regulate the output voltage, as an attempt to achieve constant power output RF energy.

Ex vivo porcine abdominal tissue with skin was selected for the experiment, and an appropriate amount of gel was adopted onto the skin area between the electrodes, which facilitated the process of heat dissipation and created

TABLE 3. Physiological Properties of the Epidermis, Dermis, Fat, Fibrous septa and Muscle [22,26–29]

Element	ε	σ (S/m)	ρ (kg/m^3)	c (J/kg·K)	k (W/m·K)	
Epidermis		0.06[a]	1200	3600	0.21	0
Dermis	4815[a]	0.4[a]	1200	3800	0.53	2.02
Fat	36.15	0.024802	850	2300	0.16	0.36
Muscle	3971.9	0.43722	1270	3800	0.53	0.47
Septa	4815b	0.4[b]	1200[b]	3800[b]	0.53[b]	0[c]

The conductivity and permittivity is the value measured at 450 kHz, and the blood perfusion is the value at the temperature of 37°C.
[a]Estimated value.
[b]Assumption.
[c]The perfusion term in the fibrous septa is neglected (Assumed fibrous septa as solid).

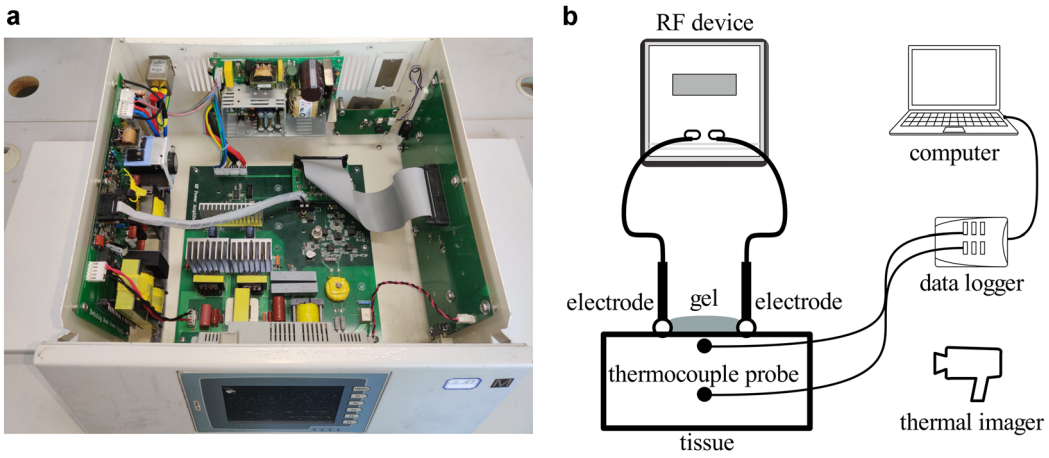

Fig. 3. (**a**) Photograph of single-channel bipolar RF device; (**b**) Schematic of the bipolar RF fat dissolution experiment. RF, radiofrequency.

moist skin with increased conductivity; the device was used to heat for 1800 seconds; two thermocouples were inserted into the tissue to plot the temperature curves of the skin layer and the fat layer at specific points and then connected to the computer via a data logger (USB-TC-08; Pico Technology, St Neots, Britain) for temperature collection; a thermal imager (870 basic; Testo, Titisee-Neustadt, Germany) was used to take the cross-sectional radiometric temperature maps of the tissue. A photograph of a single-channel bipolar RF device is shown in Figure 3a, and the schematic of the bipolar RF fat dissolution experiment is presented in Figure 3b.

RESULTS

Electric Field and Power Density Distribution

Under the electrode spacings, namely, 1, 2, and 3 cm, the power was 10 W. The distribution of the electric field and power density in the tissue are as shown in Figures 4 and 5, respectively.

The region exhibiting a higher electric field strength was distributed between the two electrodes, from the epidermis to the fat layer with a depth of nearly 4.5 mm. As the electrode spacing increased, the electric field strength in the skin area between the two electrodes decreased, and the fibrous septa and the muscle increased in the fat. At an identical depth, the electric field intensity in the fibrous septa was lower than that in the subcutaneous fat.

The direction of the current density is represented by the arrow, as shown in Figure 5, the current density in the skin area between the two electrodes was higher than that in other areas, and part of the fibrous septa exhibited a higher power density. Under the electrode spacings of 1, 2, and 3 cm, the maximal power density was located in the skin layer.

Temperature Distribution

We considered the temperature distribution of the tissue after 1800 seconds of heating at pairwise combinations with the electrode spacings of 1, 2, and 3 cm and

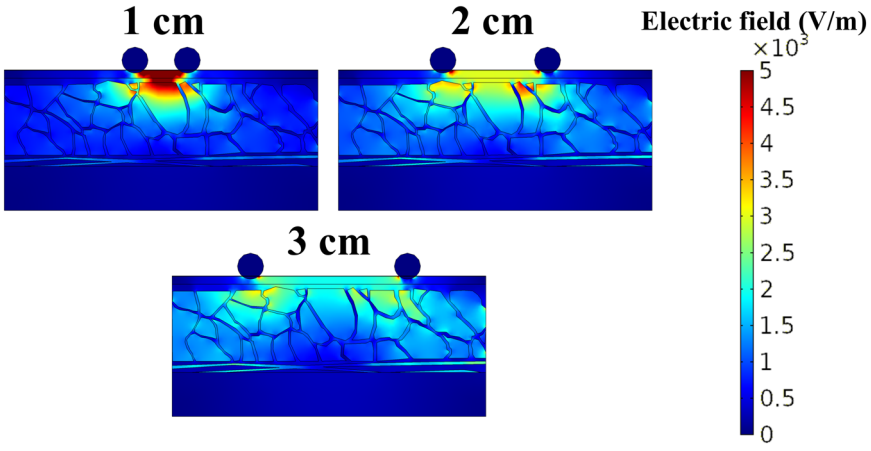

Fig. 4. The distribution of electric field in the tissue with the electrode spacing of (**a**) 1 cm; (**b**) 2 cm; and (**c**) 3 cm, respectively.

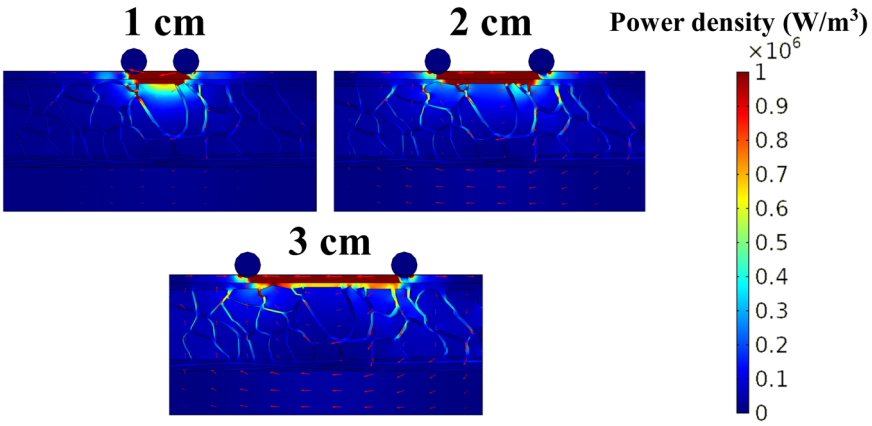

Fig. 5. The distribution of power density in the tissue with the electrode spacing of (**a**) 1 cm; (**b**) 2 cm; and (**c**) 3 cm, respectively.

power of 5, 10, and 15 W. The temperature distribution map by finite element analysis is shown in Figure 6, and by thermal imager is shown in Figure 7. The temperature profile curve by finite element analysis on $x = 0$ is plotted in Figure 8.

The temperature scale range of the temperature distribution map taken by thermal imager was consistent with the setting of finite element analysis. In contrast to the results of finite element analysis, the temperature distribution map taken by the thermal imager was not considerably different. The temperature of the part of fibrous septa was higher than the surroundings. According to Figure 8a, when the power was 5 W, and the electrode spacing was 2 or 3 cm, the profile temperature of the fat layer did not reach the condition of adipocyte apoptosis (43–45°C, maintained for 15 minutes [3]); though the maximal temperature on the profile of the fat layer was 44.87°C when the electrode spacing was 1 cm, the temperature in this area did not last long enough to cause thermal damage. Under a power of 10 W, and electrode spacing of 1 cm, part of the skin layer fell in the range of thermal damage; at the electrode spacing of 2 cm, continuous thermal damage occurred in the fat layer below the electrode, and the average temperature on the profile of the fat layer was 45.92°C, as shown in Figure 8b; while at the electrode spacing of 3 cm, thermal damage occurred in two discrete regions of the fat layer below the electrode. Under the power of 15 W, the thermal damage area in the tissue was further enlarged, and part of the skin layer was in the thermal damage area under the spacing of the three electrodes, and the maximum temperature on the profile of the fat layer reached 86.19°C at the electrode spacing of 1 cm, as shown in Figure 8c.

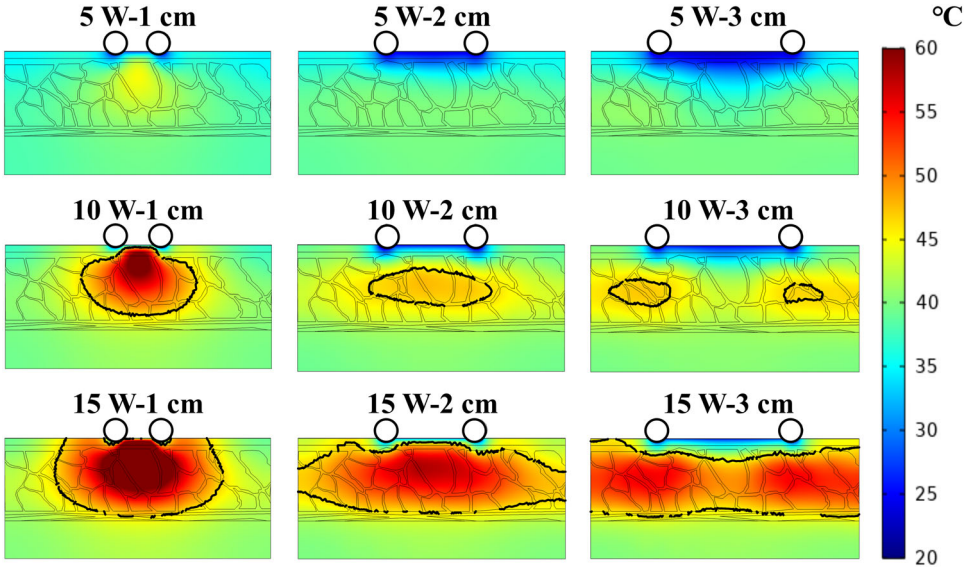

Fig. 6. Under the condition of different electrode spacings and power combinations, the distribution of temperature map by finite element analysis after heating for 1800 seconds in the tissue. Solid black lines represent the areas of the extent of irreversible thermal damage, $\Omega = 1$.

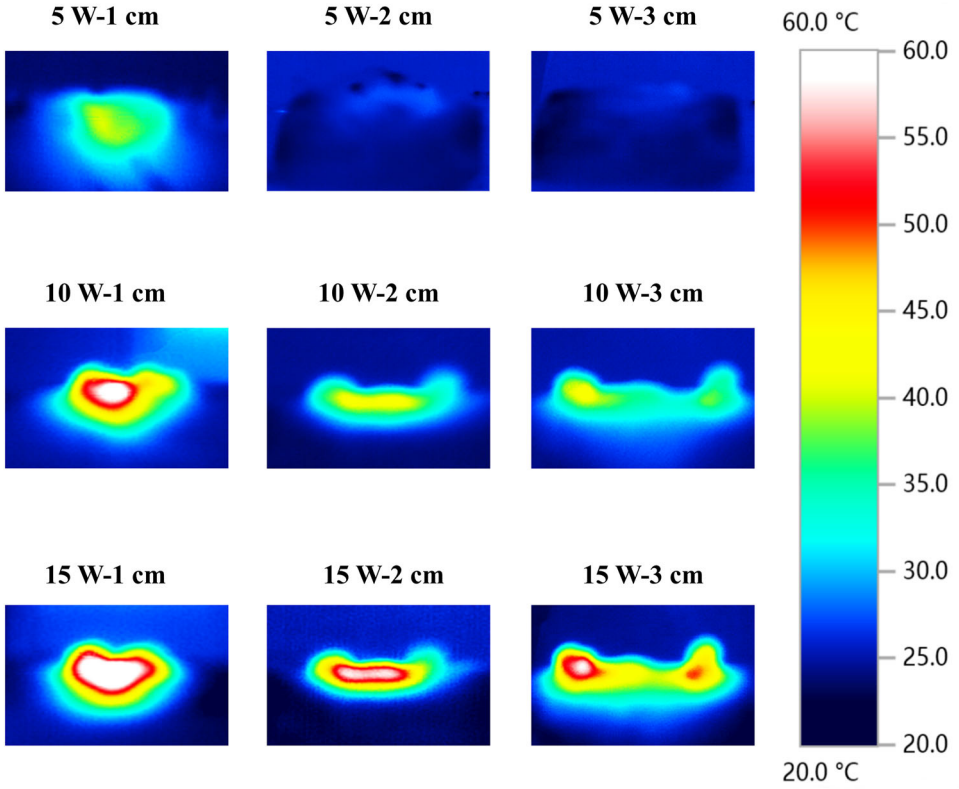

Fig. 7. Under the condition of different electrode spacings and power combinations, the distribution of temperature map by thermal imager after heating for 1800 seconds in the tissue.

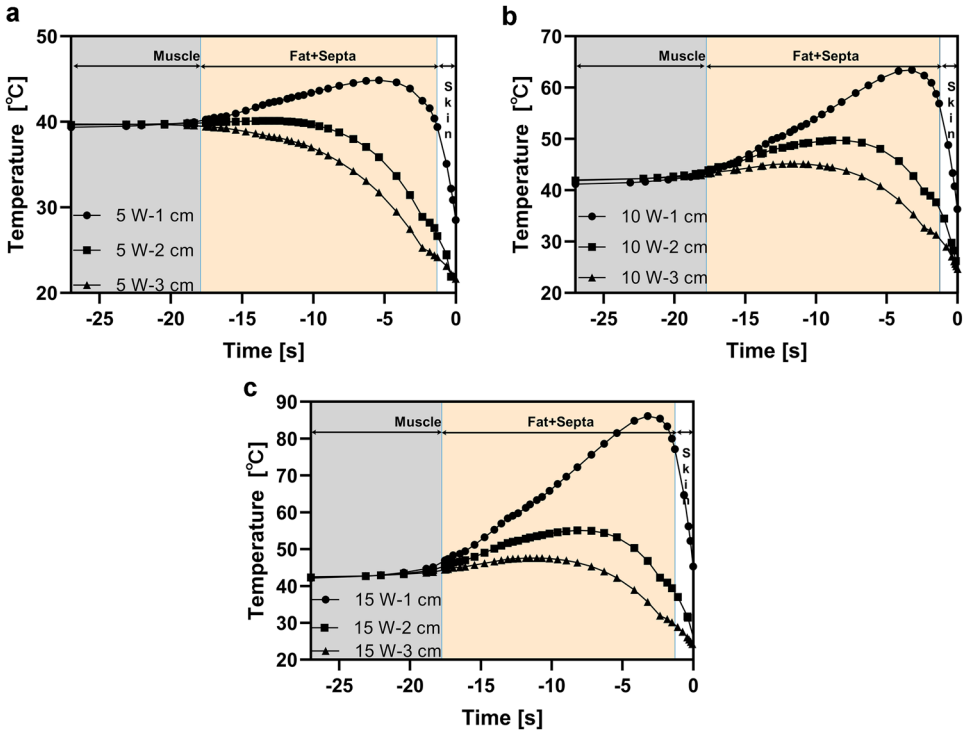

Fig. 8. Temperature profile at $x = 0$ by finite element analysis after heating for 1800 seconds in the tissue with the power of (**a**) 5 W; (**b**) 10 W; and (**c**) 15 W, respectively.

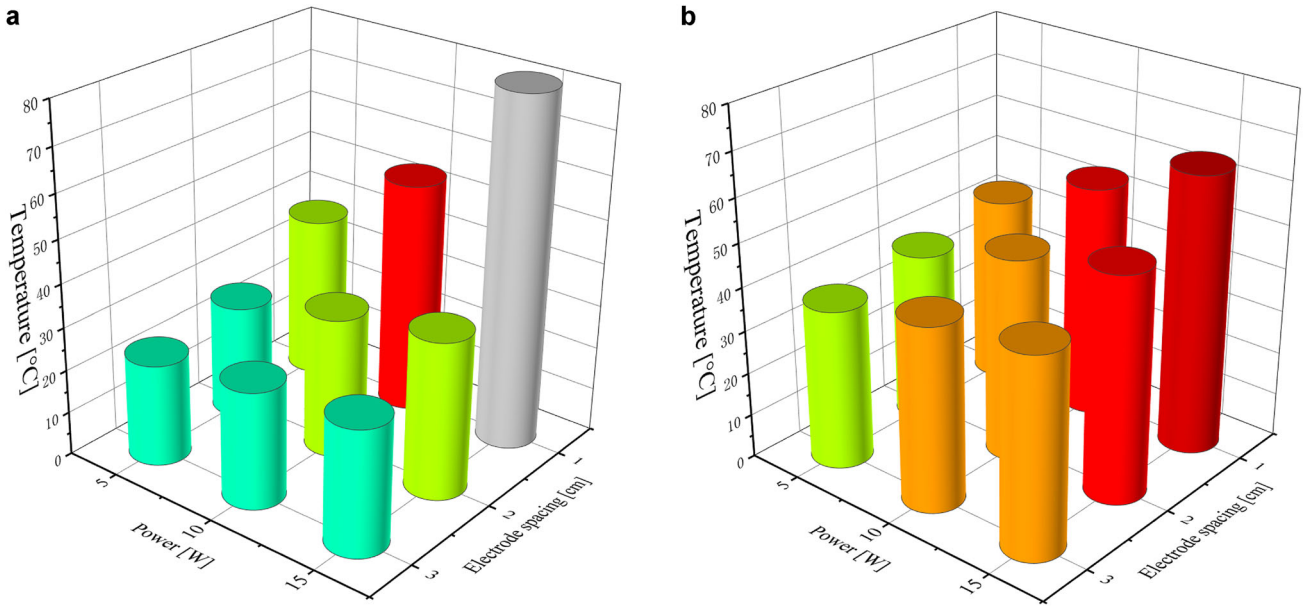

Fig. 9. Under the condition of different electrode spacings and power combinations, the temperature of the skin layer domain point probes and fat layer domain point probes by finite element analysis after tissue heating for 1800 seconds, respectively, where the x-axis represents power in W, and the y-axis represents electrode spacing in cm; the coordinates of the skin and fat layer probes in the model are (0, −1) and (0, −10), respectively. (**a**) Skin layer domain point probes; (**b**) fat layer domain point probes.

Temperature Curves at $x = 0$

Temperature curves of the domain point probe. To obtain the temperature variation trend of the skin layer and the fat layer, two domain point probes were inserted into the tissue at a depth of 1 mm (skin layer) and 10 mm (fat layer) from the epidermis at $x = 0$; the coordinates of the skin and fat layer domain point probe in the model were (0, −1) and (0, −10), respectively. Figure 9a and b present the temperature of the skin and fat layer domain point probes after tissue heating for 1800 seconds at (0, −1) and (0, −10), respectively, where the x-axis represents power in W, and the y-axis represents electrode spacing in cm. Figure 10a and b plot the temperature curves with the heating time of the domain point probe of the skin layer and fat layer at (0, −1) and (0, −10), respectively.

As shown in Figure 9a and b, the temperature of the domain point probe in the skin layer and the fat layer was positively correlated with the power while negatively associated with the electrode spacing. The electrode spacing noticeably affected the temperature of the skin domain point probe ($P < 0.05$), whereas the power had a slight effect ($P > 0.05$). Power more significantly impacted ($P < 0.01$) the

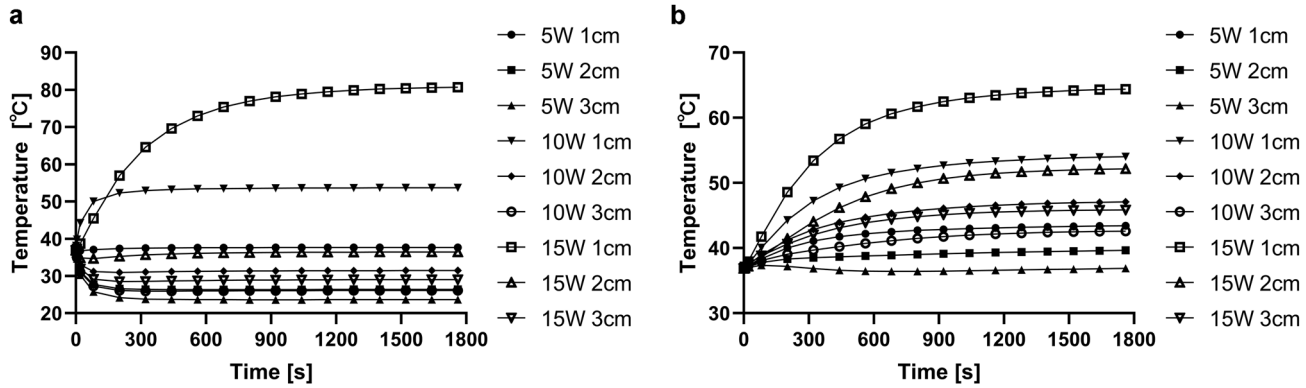

Fig. 10. Under the condition of different electrode spacings and power combinations, the curve of temperature with heating time of the skin layer domain point probes and fat layer domain point probes, respectively; the coordinates of the skin and fat domain point probes in the model are (0, −1) and (0, −10), respectively. (**a**) Skin layer domain point probes; (**b**) fat layer domain point probes.

temperature of the fat domain point probe than did electrode spacing ($0.01 < P < 0.05$). At the electrode spacing of 1 cm, and a power of 10 or 15 W, the temperature of the domain point probe in the skin layer approached to and exceeded the thermal damage threshold temperature of the skin layer (55.6°C, for blister formation [3]), respectively. Under other conditions, the temperature variation was not apparent, falling in the range of 30.39 ± 5.29°C. The temperature variation range of the fat layer point probe fell in the range of 47.37 ± 8.43°C.

As shown in Figure 10a, due to the excellent heat dissipation capacity of the gel between the two electrodes, except for the combinations of 15 and 10 W^{-1} cm, the temperature of the domain point probes in the skin layer under other combinations declined from the initial value during the RF heating and remained stable after 300 seconds; moreover, the adjacent temperature difference of the final temperature of the domain point probes in each combination was slight, falling in the range of 2.43 ± 1.59°C. Under the combination of 5 W^{-3} cm, the final temperature of the domain point probe in the skin layer declined to 23.63°C, close to the environment temperature, and it was the lowest temperature under all combinations. Unlike Figure 10a, in the temperature curve of the domain point probe in the fat layer (Figure 10b), under all combinations of electrode spacings and power, the domain point probe temperature during RF heating was close to or higher than the initial temperature, except for the combination of 15 W^{-1} cm; the adjacent temperature difference of the final temperature fell in the range of 2.47 ± 1.41°C, which was close to the adjacent temperature difference range of skin layer probes. The combination of 15 W^{-1} cm appeared to be an extreme case, causing the tissue temperature to be overly high, and the temperature of the domain point probes in the skin layer and the fat layer under this combination reached the maximal values of 80.72 and 64.4°C, respectively.

Temperature curves of the thermocouple probe. Figure 11a and b plot the temperature curves of the thermocouple probe of the skin layer and the fat layer, respectively. The insertion position of the thermocouple probe in the tissue was identical to the placement coordinates of the domain point probe in the model.

As shown in Figure 11, in the thermocouple probe temperature curves of the skin layer and the fat layer, it is difficult to ensure that the initial temperature of the tissue was 37°C but falling in the range of 36–38°C; thus, a slight difference in the initial temperature of the thermocouple probes in the tissues was identified under each combination, resulting in the phenomenon that part of the temperature curves of the thermocouple probes in the skin layer intersects at the initial stage (0–300 seconds) of RF heating. Compared with Figure 11a, the thermocouple probe in the fat layer was probably relatively far away from the RF source, causing part of the temperature curves of the thermocouple probes in the fat layer intersects to last until 600 seconds of RF heating. Combined with Figure 11a and b, the combination of 15 W^{-1} cm could also lead to excessive tissue temperature (81.51 and 65.08 °C, respectively) in the practical *ex vivo* experiment.

Compared with the temperature curves of the domain point probe, under the combination of the identical power and electrode spacing, the average temperature difference between the two at 1800 seconds of heating was 0.605°C (skin layer probe) and 0.815°C (fat layer probe), respectively; the temperature trend of the two was similar, tending to stabilize after about 300 seconds (skin layer probe) and 1200 seconds (fat layer probe), respectively, and the temperature variation in the residual time was less than 1°C. Significantly different from the temperature trend of the domain point probe, under a power of 15 W and a electrode spacing of 1 cm, the temperature curves of the thermocouple probes in the skin layer and the fat layer continued to rise steadily at the rates of 7.92E−3 and 4.1E−3 °C/s until 1800 seconds, respectively.

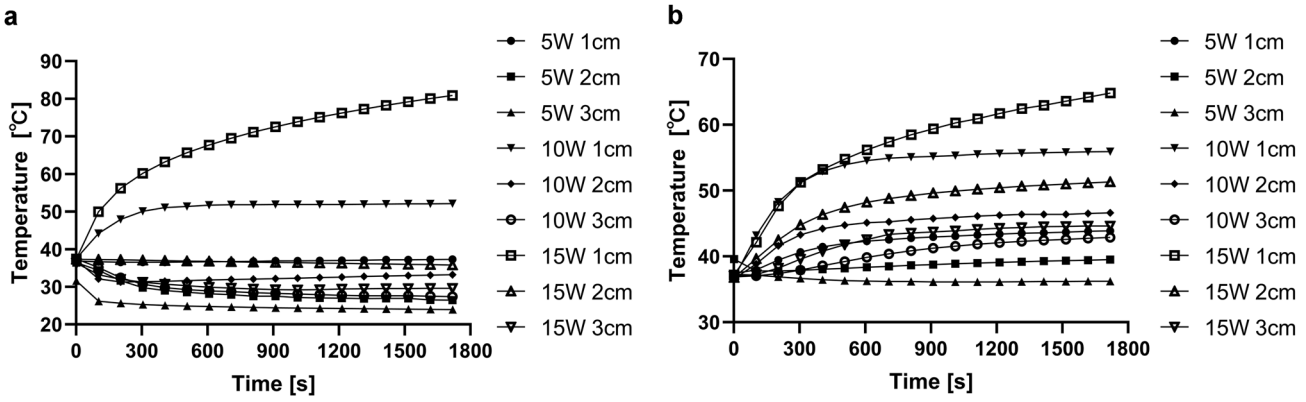

Fig. 11. Under the condition of different electrode spacings and power combinations, the curve of temperature with heating time of the skin layer thermocouple probes and fat layer thermocouple probes, respectively; the coordinates of the skin and fat layer thermocouple probes in the ex vivo tissue are (0, −1) and (0, −10), respectively. (**a**) skin layer thermocouple probes; (**b**) fat layer thermocouple probes.

The above mentioned finding was probably because a series of physiological structural variations and blood coagulation occurring after death. When the temperature in the tissue was low, the effect of blood perfusion on the tissue heat dissipation was relatively slight, whereas, at the overly high tissue temperature, the lack of blood perfusion led to the accumulation of heat in the tissues, probably resulting in the continuous rise of the thermocouple temperature in the experiment.

Temperature Curves at Thermal Damage Area

This study suggests that under a power of 10 W, an electrode spacing of 2 or 3 cm could produce irreversible thermal damage area in the fat layer; in the meantime, RF energy did not thermally damage the skin layer. Franco et al. [3] proposed that 15 minutes thermal exposures to 43–45°C cause a delayed adipocyte cellular death response. To investigate whether the temperature in the thermal damage area caused by these two reasonable fat dissolution configurations can satisfy the mentioned temperature requirements, the coordinates of the domain point probe placed in the model was altered to (−12.5, −10), thereby locating the domain point probe in the thermal damage area of the fat layer caused by combinations of $10\,W^{-2}$ cm and $10\,W^{-3}$ cm. Three *ex vivo* porcine abdominal tissues with the skin were taken for the experiment, and the thickness of the fat layer of the tissues was measured as falling in the range of 17.3 ± 0.5 cm, close to the thickness of the fat layer in the finite element model of the tissues. The insertion position of the thermocouple probe in the tissue was identical to the placement coordinates of the domain point probe in the model.

Figure 12 shows the comparison between the temperature curves of the domain point probe and that of the thermocouple probe in the thermal damage area of the model and the *ex vivo* tissue in RF heating under a combination of $10\,W^{-2}$ cm and $10\,W^{-3}$ cm. According to Figure 12, after heating for 1800 seconds, under the combination of $10\,W^{-2}$ cm, the final temperature of the domain point probe in the model and the thermocouple probes in the *ex vivo* experiment were correspondingly higher by nearly 0.7°C in the combination of $10\,W^{-3}$ cm. The temperature curves of each combination of the domain point probes and the thermocouple probes fitted closely. During RF heating, the maximum temperature difference between the domain point probe and the thermocouple probe of each combination occurred at the end of heating, and the temperature difference reached 0.38 and 0.47°C, respectively, corresponding to the combination of $10\,W^{-2}$ cm and $10\,W^{-3}$ cm. The combinations of $10\,W^{-2}$ cm and $10\,W^{-3}$ cm reached 43°C in RF heating after about 600 and 900 seconds, respectively, both being higher than 43°C during the subsequent heating. Thus, both combinations could maintain the temperature at the location of the domain point probe and thermocouple probe above 43°C for at least 15 minutes.

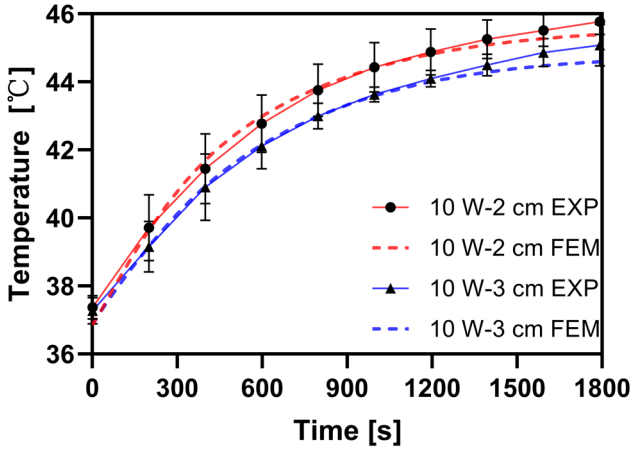

Fig. 12. Under the combination of $10\,W^{-2}$ cm and $10\,W^{-3}$ cm, the curve of temperature with heating time of the domain point probes and thermocouple probes in the thermal damage area of the model and the ex vivo tissue, respectively; the coordinates of the domain point probes and thermocouple probes in the model and in the *ex vivo* tissue both (−12.5, −10).

Strictly speaking, though this conclusion can only represent the temperature curve of a specific location in the thermal damage area, as this specific location should only be in the intersection of the thermal damage region caused by the combinations of $10\,W^{-2}$ cm and $10\,W^{-3}$ cm, it can be considered that the location of domain point probes and thermocouple probes has a certain degree of randomness; moreover, Figure 6 shows that the temperature distribution in the thermal damage area was relatively uniform under the combination of $10\,W^{-2}$ cm and $10\,W^{-3}$ cm. In brief, it may be considered that the temperature curve of the domain probe and thermocouple in Figure 12 can represent the general situation of the whole thermal damage region, that is, the temperature in the thermal damage area caused by the fat dissolution configuration of $10\,W^{-2}$ cm and $10\,W^{-3}$ cm may satisfy the fat dissolution temperature requirements.

DISCUSSION

Given the above finite element analysis results and *ex vivo* experimental results, the effects of RF energy on the electrical and thermal aspects of biological tissues at nine different combinations of power and electrode spacing were ascertained.

As the physical properties of the tissue were constant, the power density of the tissue at specific locations was determined by the internal electric field, which, in turn, was ascertained by the morphology of the tissue. For the individual fibrous septa, the intensity of the electric field varied with the direction and position of the septa relative to the incident electric field. In the bipolar RF model built here, the direction of the electric field in the tissue was an arc shape from electrode “b” to electrode “a.” The fibrous septa parallel to the electric field constitute the path of less resistance with enhanced electric flux, thereby leading to a stronger internal electric field. In contrast, the intensity of the electric field in the fibrous septa

perpendicular to the electric field was relatively low [11]. According to equation 2, the energy dissipation rate per unit volume at a given point was proportional to the electric conductivity of the tissue and the square of the induced internal electric field, probably accounting for the fact that the power density of part of fibrous septa is higher than the surrounding ones.

Permittivity refers to a measure of the ability of the material dipoles to rotate or its charge to be stored by an applied external electric field [23]. The values of permittivity of fat and fibrous septa, fat = 36.15 and fibrous septa = 4815 at an applied RF frequency of 450 kHz indicated that fibrous septa were more easily polarized than fat; thus, the fibrous septa were less resistive to the electric flux. As the current circulated through the fibrous septa and the fat, the voltage inside the fat declined even more. By definition, the electric field is equal to the negative gradient of the electric potential, so the strength of the electric field in the fat was higher than in the fibrous septa in total. The electric conductivity of fibrous septa followed an order of magnitude larger than that of the fat; in the meantime, as the electric field for the individual fibrous septa is determined by its position relative to the direction of the electric field, given the above factors, the fibrous septa parallel to the direction of the electric field would produce the maximum power density, followed by the fat lobule. Moreover, the fibrous septa perpendicular to the direction of the electric field exhibited the minimum power density. Areas with higher power absorption corresponded to higher heating, probably explaining the reason why the temperature of part of fibrous septa was higher than the surroundings.

The power density of the fibrous septa at different locations and the fat lobules led to a significant temperature gradient between them under RF heating, the fibrous septa parallel to the electric field was the primary heat source of subcutaneous tissue. It was preferentially heated, and then the heat flux diffused towards the adjacent fat lobules. Thus, the fibrous septa helped increase the temperature of the subcutaneous fat under RF heating. Ana et al. [15] simulated the situation of subcutaneous fat tissue with fibrous septa and homogeneous subcutaneous fat tissue under RF heating for 8000 seconds, respectively; they reported that the maximum temperature of the former was 4°C higher than that of the latter in the steady-state.

The power density was determined by the current density and the electric field intensity. Though the current density in the subcutaneous fat layer was relatively lower, the characteristic of the fat layer as a poor conductor of electricity made its electric field higher; the fibrous septa helped increase the electric field range and intensity in the subcutaneous fat layer [11], probably causing the power density generated in the part of the fat layer area to be relatively high. The position of the skin layer close to the electrode led to a tremendous electric field intensity in this area; in the meantime, for its excellent electrical conductivity, the current density of the skin layer was relatively high, so the skin layer exhibited the maximum power density. According to the above mentioned electrical analysis, the skin layer and part of the fat layer were the main temperature rise area during RF heating.

Heat conduction in the tissue consists of blood perfusion, heat conduction, and electrical absorption. As shown in Figures 6 and 7, at a close electrode spacing, the skin layer and the fat layer had a denser lateral current and were preferentially heated; and with the increase in electrode spacing and heating time, the transverse current flow area between the two electrodes was extended downward, making the fat layer start to heat up on a large scale; at an electrode spacing further enlarged, for the excellent heat dissipation property of the gel between the two electrodes, the temperature in the area under the gel was lower than the temperature of the surrounding tissue. At an identical electrode spacing, the increase in power made the average temperature in the tissue higher, leading to the expansion of the thermal damage area. This study suggests that under the condition of nine different combinations of power and electrode spacings, the distribution of heat in tissues varied significantly. It was reported here that the combination of $10\,W^{-2}$ cm and $10\,W^{-3}$ cm could produce an irreversible thermal damage area in the fat layer, and the temperature in the thermal damage area could meet the fat dissolution temperature requirements; in the meantime, the RF energy did not thermally damage the skin layer. By COMSOL's built-in integral calculation, the area of thermal damage area was found to be $1.7254\,cm^2$ under the combination of $10\,W^{-2}$ cm, and $0.7912\,cm^2$ under the combination of $10\,W^{-3}$ cm, the former being 118% larger than the latter. For bulged skin nodules, RF energy was not expected to thermally damage the normal fat area during treatment; the combination of a power of 10 W and electrode spacing of 3 cm might be more suitable since it could cause discontinuous thermal damage to the fat layer.

This study defined a heat dissipation coefficient to simulate the cooling effect generated by gel. According to the temperature profile curve of $x = 0$ (Figure 8), the temperature of the skin layer was lower than the fat layer near the skin layer, indicating that the temperature rise of the skin layer was suppressed to some extent. However, at a too small electrode spacing (1 cm) or if the power was too high (15 W), RF energy would still thermally damage the skin layer around the electrodes. The reason for the above mentioned finding might be that the heating effect of RF on the skin layer was far beyond the cooling ability of the gel, resulting in excessive heat accumulation in the skin layer. To avoid thermal skin damage in the loading of higher power RF energy to tissues, more effective heat dissipation methods should be adopted (e.g., placing a cooling plate on the surface of the skin that provides a constant temperature [3]).

Several clinical types of research demonstrated the feasibility of different bipolar RF devices for fat dissolution. For instance, Mario et al. [24] used a ThermaLipo™ RF bipolar pulsed emission device (Thermamedic Ltd., Alicante, Spain) to conduct 45 minutes RF treatment on 30 women, during which the skin temperature was maintained between 40

and 42°C; the histological findings observed in biopsies of cellulite suggested that adipocytes were more polyhedric, with irregular, degenerated membranes, and with less or no lipid content and apoptotic variations. Sylvie et al. [25] used a novel RF device (BodyFX; InMode Inc., Yokneam, Israel) which utilized a suction-coupled bipolar RF configuration, to treat twenty-one subjects for their abdominal fat once weekly for 6 weeks, a single 10 minutes treatment for each zone, the skin surface cut off temperature was set at 42°C; histologically, adipocytes were observed to exhibit decreased sizes and withered shapes, with elevated levels of apoptosis; Significant clinical improvements ($P < 0.05$) were observed for the following clinical outcomes (e.g., reduction of abdominal circumference, subcutaneous adipose tissue thickness, and in adipose tissue weight) at 3-month follow-up visits. However, the parameters of these devices (e.g., power, electrode spacing, and RF frequency) varied to some extent, and no uniform standards have been reached thus far. It seems that more studies are required to develop reasonable parameters for bipolar RF fat dissolution from an engineering perspective.

CONCLUSION

Different electrode spacings and power combinations significantly affect the electrical and thermal properties of bipolar RF energy loaded on biological tissue, a reasonable electrode spacing and power combination is one of the critical factors leading to the success of bipolar RF fat dissolution. According to the results of finite element analysis and *ex vivo* experiment, the combination of a power of 10 W and electrode spacing of 2 or 3 cm enables the fat layer of the tissue to satisfy the requirements of fat dissolution, and the fat dissolution area caused by the former was 118% larger than that of the latter.

ACKNOWLEDGMENTS

The author would like to express his sincere gratitude to Dr. Franco for providing the method of extracting realistic fibrous septa configuration from micro-MRI Images via email.

REFERENCES

1. Mulholland RS, Paul MD, Chalfoun C. Noninvasive body contouring with radiofrequency, ultrasound, cryolipolysis, and low-level laser therapy. Clin Plast Surg 2011;38(3):503–520.
2. Weiss RA. Noninvasive radio frequency for skin tightening and body contouring. Semin Cutan Med Surg 2013;32(1):9–17.
3. Franco W, Kothare A, Ronan SJ, Grekin RC, McCalmont TH. Hyperthermic injury to adipocyte cells by selective heating of subcutaneous fat with a novel radiofrequency device: feasibility studies. Lasers Surg Med 2010;42(5):361–370.
4. Kaplan H, Gat A. Clinical and histopathological results following TriPollar radiofrequency skin treatments. J Cosmet Laser Ther 2009;11(2):78–84.
5. Anolik R, Chapas AM, Brightman LA, Geronemus RG. Radiofrequency devices for body shaping: A review and study of 12 patients. Semin Cutan Med Surg 2009;28(4):236–243.
6. Friedmann DP. A review of the aesthetic treatment of abdominal subcutaneous adipose tissue: Background, implications, and therapeutic options. Dermatol Surg 2015; 41(1):18–34.
7. Sadick NS, Makino Y. Selective electro-thermolysis in aesthetic medicine: A review. Lasers Surg Med 2004;34(2):91–97.
8. Araujo AR, Soares VP, Silva FS, Moreira Tda S. Radiofrequency for the treatment of skin laxity: Mith or truth. An Bras Dermatol 2015;90(5):707–721.
9. Doss JD. Calculation of electric fields in conductive media. Med Phys 1982;9(4):566–573.
10. MIT. Steady Ohmic Conduction. http://web.mit.edu/6.013_book/www/chapter7/7.2.html. Accessed March 13, 2020.
11. Jimenez Lozano JN, Vacas-Jacques P, Anderson RR, Franco W. Effect of fibrous septa in radiofrequency heating of cutaneous and subcutaneous tissues: Computational study. Lasers Surg Med 2013;45(5):326–338.
12. Pennes HH. Analysis of tissue and arterial blood temperatures in the resting human forearm. J Appl Physiol 1985;85(1):5–34.
13. Berjano EJ. Theoretical modeling for radiofrequency ablation: State-of-the-art and challenges for the future. Biomed Eng Online 2006;5(1):24.
14. Mirrashed F, Sharp JC, Krause V, Morgan J, Tomanek B. Pilot study of dermal and subcutaneous fat structures by MRI in individuals who differ in gender, BMI, and cellulite grading. Skin Res Technol 2004;10(3):161–168.
15. Gonzalez-Suarez A, Gutierrez-Herrera E, Berjano E, Jimenez Lozano JN, Franco W. Thermal and elastic response of subcutaneous tissue with different fibrous septa architectures to RF heating: Numerical study. Lasers Surg Med 2015;47(2):183–195.
16. Henriques FC, Moritz AR. Studies of thermal injury: I. The conduction of heat to and through skin and the temperatures attained therein. A theoretical and an experimental investigation. Am J Pathol 1947;23(4):530–549.
17. Moritz AR, Henriques FC. Studies of thermal injury: II. The relative importance of time and surface temperature in the causation of cutaneous burns. Am J Pathol 1947;23(5): 695–720.
18. Xu F, Lu T. Introduction to Skin Biothermomechanics and Thermal Pain. Berlin, Heidelberg: Science Press Beijing and Springer-Verlag; 2011. p 48.
19. Xu F, Lu TJ, Seffen KA, Ng EYK. Mathematical modeling of skin bioheat transfer. Appl Mech Rev 2009;62(5): 050801–050135.
20. Haemmerich D, Schutt DJ, dos Santos I, Webster JG, Mahvi DM. Measurement of temperature-dependent specific heat of biological tissues. Physiol Meas 2005;26(1):59–67.
21. Bhattacharya A, Mahajan RL. Temperature dependence of thermal conductivity of biological tissues. Physiol Meas 2003;24(3):769–783.
22. Kengne E, Lakhssassi A, Vaillancourt R. Temperature distribution in living biological tissue simultaneously subjected to oscillatory surface and spatial heating: analytical and numerical analysis. Int J Math Forum 2012;7(48):2373–2392.
23. Miklavčič D, Pavšelj N, Hart FX. Electric properties of tissues. Wiley Encyclopedia of Biomedical Engineering. New York, NY: John Wiley & Sons; 2006. p 2.
24. Trelles MA, van der Lugt C, Mordon S, Ribe A, Al-Zarouni M. Histological findings in adipocytes when cellulite is treated with a variable-emission radiofrequency system. Lasers Med Sci 2010;25(2):191–195.
25. Boisnic S, Divaris M, Nelson AA, Gharavi NM, Lask GP. A clinical and biological evaluation of a novel, noninvasive radiofrequency device for the long-term reduction of adipose tissue. Lasers Surg Med 2014;46(2):94–103.
26. Wilson SB, Spence VA. A tissue heat transfer model for relating dynamic skin temperature changes to physiological parameters. Phys Med Biol 1988;33(8):895–912.
27. Gabriel C. Dielectric Properties of Body Tissues in the frequency range 10 Hz–100 GHz. http://niremf.ifac.cnr.it/tissprop/. Accessed March 13, 2020.
28. Wake K, Sasaki K, Watanabe S. Conductivities of epidermis, dermis, and subcutaneous tissue at intermediate frequencies. Phys Med Biol 2016;61(12):4376–4389.
29. Tsai B, Xue H, Birgersson E, Ollmar S, Birgersson U. Dielectrical properties of living epidermis and dermis in the frequency range from 1 kHz to 1 MHz. J Elec Bioimp 2019;10(1):14–23.